

Cartography and Geographic Information Science



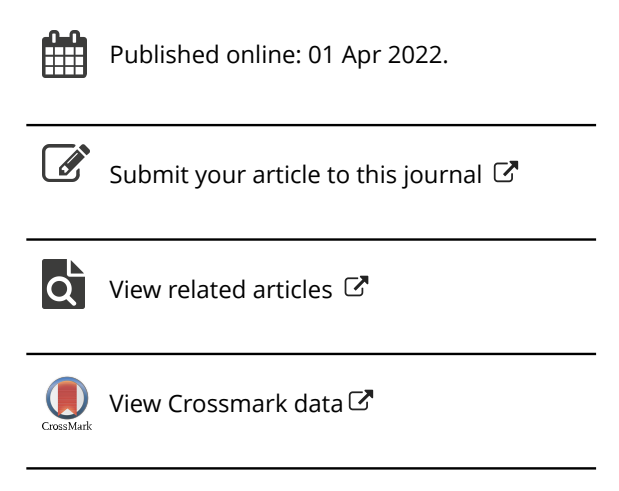
ISSN: (Print) (Online) Journal homepage: https://www.tandfonline.com/loi/tcag20

Analyzing multi-scale spatial point patterns in a pyramid modeling framework

Yi Qiang, Barbara Buttenfield & Jinwen Xu

To cite this article: Yi Qiang, Barbara Buttenfield & Jinwen Xu (2022): Analyzing multi-scale spatial point patterns in a pyramid modeling framework, Cartography and Geographic Information Science, DOI: 10.1080/15230406.2022.2048419

To link to this article: https://doi.org/10.1080/15230406.2022.2048419





ARTICLES



Analyzing multi-scale spatial point patterns in a pyramid modeling framework

Yi Qiang (Da, Barbara Buttenfield (Db) and Jinwen Xu (Da)

^aSchool of Geosciences, University of South Florida, Tampa, FL, USA; ^bDepartment of Geography, University of Colorado – Boulder, Boulder, CO, USA

ABSTRACT

Many spatial analysis methods suffer from the scaling issue identified as part of the Modifiable Areal Unit Problem (MAUP). This article introduces the Pyramid Model (PM), a hierarchical data framework integrating space and spatial scale in a 3D environment to support multi-scale analysis. The utility of the PM is tested in examining quadrat density and kernel density, which are commonly used measures of point patterns. The two metrics computed from a simulated point set with varying scaling parameters (i.e. quadrats and bandwidths) are represented in the PM. The PM permits examination of the variation of the density metrics computed at all different scales. 3D visualization techniques (e.g. volume display, isosurfaces, and slicing) allow users to observe nested relations between spatial patterns at different scales and understand the scaling issue and MAUP in spatial analysis. A tool with interactive controls is developed to support visual exploration of the internal patterns in the PM. In addition to the point pattern measures, the PM has potential in analyzing other spatial indices, such as spatial autocorrelation indicators, coefficients of regression analysis and accuracy measures of spatial models. The implementation of the PM further advances the development of a multi-scale framework for spatio-temporal analysis.

ARTICLE HISTORY

Received 5 August 2021 Accepted 27 February 2022

KEYWORDS

MAUP; multi-scale analysis; point pattern; kernel density; quadrat density; visualization

1. Introduction

Multi-scale analysis of spatial pattern is a longstanding challenge in GIScience. Analyses conducted at different spatial scales often create different results. The importance of scale in spatial analysis has been epitomized in the well-known Modifiable Areal Unit Problem (MAUP) (Openshaw 1983). Ideally, spatial data should be analyzed at the level where spatial processes become evident, are best understood and/or where spatial relationships are maximized (Lam 1983; Wagner and Fortin 2005). However, most spatial analyses and modeling are conducted at a pre-defined scale or the scale where data is collected, which may miss critical processes and relationships concealed at other scales. Currently, the increasing diversity of geospatial data collected at different resolutions (e.g. satellite, UAV, and field-survey data) poses challenges for data integration and model coupling in existing GIS platforms and spatial analysis tools. Given the complex and multi-scale nature of big geospatial data, there is a pressing need for developing novel modeling frameworks and analytical tools to understand the multiscale processes and relationships in various geographical phenomena.

The challenge of multi-scale analysis can be attributed to the traditional presentation of geospatial data. In prevalent geographic information systems (GIS), space is conventionally represented in "flat layers" and spatial analysis tools usually operate at a single scale. For instance, with a predefined bandwidth, kernel density can detect clusters of spatial features at a certain scale. To examine the clustering patterns at other scales, the bandwidth needs to be adjusted, often using a "trial-and-error" approach. Such snapshots of spatial patterns at discrete scales are inefficient and inconsistent in showing variation of spatial patterns across scales. Additionally, the patterns of focal statistics (e.g. mean and standard deviation) and local spatial indicators (e.g. spatial autocorrelation) may vary with the size of a moving window. Spatial modeling tasks (e.g. image classification and land cover change modeling) often incorporate neighborhood conditions within such moving windows (Chica-Olmo & Abarca-Hernández, 2000; Wu, 2002). However, the choice of window size is often subjectively determined, leading to modeling results that only capture spatial relation at a single scale. A common solution to this issue is repeating the analysis at a few selected scales or

2 🕒 1. Q.....

different sizes of moving windows. Discrete sampling in the scale dimension cannot fully uncover the continuous variation of spatial pattern across different scales.

Analytical tools and modeling frameworks have been developed to detect spatial patterns at multiple scales and measure the scales of processes underlying observed geographic phenomena. Notable work includes Multiscale Geographically Weighted Regression (MGWR) developed by (Fotheringham et al., 2017), which relaxes the GWR's assumption of single bandwidth by allowing it to vary among predictive variables. Some cluster detection techniques, such as DBSCAN (Ester et al., 1996) and Kulldorff's scan statistic (Kulldorff, 1997), can detect spatial clusters of various shapes and sizes. The detected clusters may signal spatial processes operating at different scales but fail to reveal the hierarchy and nested relations between multiscale processes. Additionally, a variogram is a common metric used to measure the scale of spatial dependence (Behrens et al., 2019) and neighborhood effect (Lam et al., 2018). The range in a variogram indicates the scale range within which a variable is spatially autocorrelated. Another notable example occurs when aggregating spatial data into areal units. The scale effect may invoke the Modifiable Areal Unit Problem (MAUP), which refers to the phenomena that analysis conducted in different sizes (scale) and shapes (zoning) of spatial units may lead to different results. MAUP in different types of analysis has been extensively investigated in the literature (e.g. Ye, 2021; Ye & Rogerson, 2021). To mitigate MAUP in spatial analysis, Chen et al. (2019) used a nugget-sill ratio in semi-variograms as an indicator to determine the optimal scale for spatial aggregation. Duque et al. (2018) introduced a nonparametric statistical test (S-maup) to measure the sensitivity of spatial variables to the effect of MAUP.

The research on MAUP increases our understanding about the scale effect in spatial analysis and provides actionable tools to identify optimal scales for spatial analysis and modeling. Existing multi-scale analysis approaches tend to treat space and scale as two separate variables. They either analyze changes of a spatial metric at different scales (e.g. comparing semi-variogram at multiple scales) or compare scales of spatial processes at different locations (e.g. MGWR). However, the existing approaches cannot fully reveal hierarchical structures and nested relations between spatial processes at different scales. The solution to this challenge requires a modeling framework that can seamlessly integrate space and scale to represent spatial metrics varying in both location and scale. Despite advances in data models that couple traditional views of space and time

(Hägerstraand, 1970; Kraak, 2003; Miller, 1991), tight couplings of spatial data across progressions of scale are at present limited to indirect or inferential methods. Recently, Qiang et al. (2014) developed a multi-scale temporal model and subsequently extended it into a Pyramid Model (PM) that integrates spatial location and spatial scale in a true 3D space (Qiang et al., 2018; Qiang & Van de Weghe, 2019). The PM affords the opportunity to directly link spatial patterns across scale but has not yet been applied to analytic tasks. This paper demonstrates that the PM seamlessly integrates space and scale in a 3D tool that supports simultaneous monitoring and assessment of spatial patterns across a range of scales. By extending conventional spatial statistical methods to operate within the PM framework, this paper undertakes that challenge, modifying conventional spatial analytic tools for multi-scale point pattern analysis. The contribution of the work is to demonstrate how the PM implementation offers insights about density variation and cluster emergence across spatial scales that are not directly available when such analyses are conducted at individual or discrete processing scales.

The remainder of the article is organized as follows. First, common methods for density-based point pattern analysis are reviewed, and the scale issues in these methods are discussed. Next, the PM is introduced as well as relevant model variants in the multi-scale analysis framework. Then, kernel density and quadrat density metrics are implemented in the PM. Application to density estimation and point clustering is demonstrated for a synthetic dataset to explore the types of interpretations and insights that can be gained. Finally, the findings and contributions of this study will be discussed, and future work will be proposed.

2. Density-based point pattern analysis

2.1. Quadrat density

Quadrat density is a density-based measure of point pattern, which divides the space into sub-regions (i.e. quadrats) and computes the point density in each quadrat (O'Sullivan & Unwin, 2010; Yuan et al., 2020). For example, in Figure 1(b), the study area is divided into uniformly shaped quadrats, and point density in each quadrat is the ratio between total points and quadrat area. In addition, quadrats can take different shapes, such as hexagons, squares, triangles, and Voronoi polygons. Despite the simplicity in computing and interpretation, quadrat density analysis seriously suffers from the Modifiable Areal Unit Problem (MAUP). The analysis result is highly sensitive to the size of the quadrat

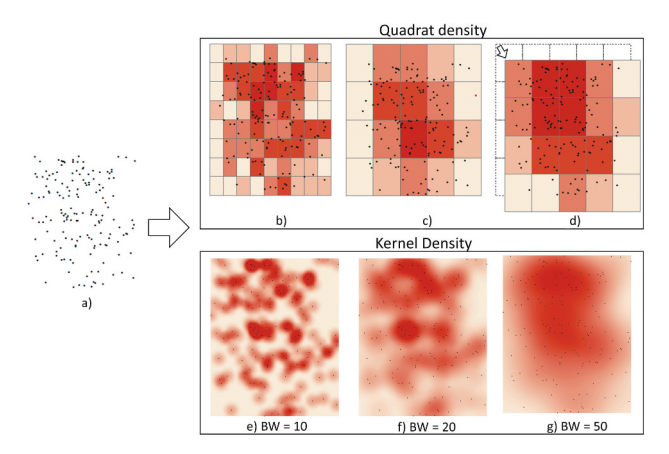


Figure 1. Pattern variations of quadrat density and kernel density at different scales. a) a simulated point set. b) point density in small quadrats. c) point density in large quadrats. d) point density in large quadrats with shifted position. e) – g) kernel density maps with different bandwidths (BW: bandwidth).

and only reflects point patterns at a single scale. A small quadrat size can detect subtle point clusters at a local scale (Figure 1(b)), but mask out general patterns at a coarser scale. A large quadrat size does the opposite: detecting coarse-scale density patterns while missing subtle clusters at local scales (Figure 1(c)). Even with the same quadrat size, the analysis result may differ if the alignment of the quadrat changes (Figure 1(d)). In most studies, the choice of quadrat size, shape, and arrangement is based on subjective decisions. Uniform quadrats may not equally fit the entire data sets in which clustering patterns are prominent at different scales.

2.2 Kernel Density

Whereas quadrat density simply counts points within quadrat cells, kernel density develops a continuous surface that can aid the detection of clusters and "hot spots" where spatial point patterns are concentrated. A kernel function is applied to each point, measuring the point density within the kernel "envelope." In addition to the number of points in a kernel, the distance from other points is taken into account, allowing the kernel to take on various shapes and sizes (Yin, 2020). The surface is generated by aggregating individual kernel functions. In GIS, the most commonly used are the quartic function (biweight) and Gaussian function, both of which can create a relatively smooth density surface. The shape of the kernel is determined by the bandwidth h, which is the scaling or smoothing factor for kernel density maps. Larger *h* creates more widespread kernels. Thus, kernel density functions with a larger h are smoother and can highlight general patterns at a coarser scale, while a smaller h can detect clusters at a finer (local) scale.

Despite the importance of h, there is no general consensus on the choice of h for a particular dataset, although specific disciplines tend to adopt specific fixed estimation methods (see, for example, Diggle et al. (2005) or Gatrell et al. (1996) for spatial epidemiology). In most cases, users either arbitrarily set a fixed value for h based on their experience, or use the Silverman's "rule-of-thumb" bandwidth (Silverman, 1986) in spite of cautionary assumptions about applying this method for non-Gaussian distributions. However, a fixed bandwidth may not perform equally well in local areas, as it may undersmooth areas with sparse features and oversmooth high-density areas. To address this issue, adaptive kernel estimators are developed to apply varying *h* over space according to the local density (Mills, 2011; Van Kerm, 2003). Tiwari and Rushton (2005, 2010) demonstrated that spatially adaptive kernel can equalize the variance in estimated density while maximizing the amount of geographic details portrayed on the map. In addition to the interpretation difficulties for maps created by adaptive estimators, there are also debates on whether the adaptive kernel estimators really bring advantages with the extra computational complexity (Terrell & Scott, 1992).

Regardless of how the bandwidth is determined, kernel density surfaces are often mapped to visualize the clusters as a "heat map" (Figure 1(e-g)). Using existing (fixed or adaptive) methods, a kernel density map only represents density estimation at a single scale at each location. In a single map, it is impossible to observe the evolving spatial pattern across multiple scales, or how the local clusters at local scales converge or cancel each other at coarser scales. The PM is proposed as a method to overcome the single-scale limitation for either quadrat or kernel density by organizing a framework linking density estimates across scales.

3. The pyramid model framework

In the PM, each point represents a specific spatial unit (a pixel) in geographic space. The horizontal position (x, y) of the point represents the spatial location of the unit, which is usually defined as the centroid of the unit. The vertical position (z) indicates the size of the unit (Figure 2). Using raster data as an example, the spatial units at the finest resolution are pixels, which are represented as points at the lowest level of the pyramid. Points at the second level represent the aggregation of spatial units in a window (2 \times 2 pixels). Points at the nth level represent windows of $n \times n$ pixels. In such a way, windows of progressive sizes are projected onto a lattice of points in the 3D space, where the (x,y)

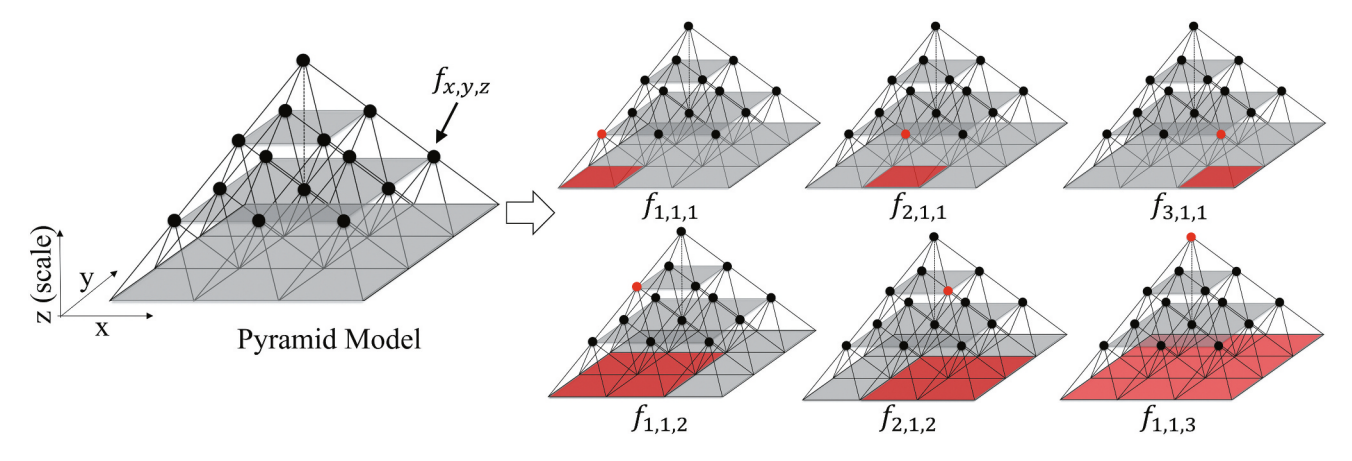


Figure 2. Conceptual framework of PM.

coordinates of a point represent the horizontal position of the centroid of each window, and z represents the size of the window. Points at the same z level may represent overlapping windows of the same size (e.g. $f_{1,1,2}$ and $f_{2,1,2}$ in Figure 2), which overcomes the limitation of non-overlapping aggregation in quadrat density. Not limited to square shape, the windows can be other circles or hexagons but have to remain consistent within a PM.

Each point in the 3D point lattice is associated with a spatial index $(f_{x,y,z})$ computed in the window the point represents. The index $f_{x,y,z}$ can represent a summary statistic (e.g. mean, standard deviation or density), or a spatial autocorrelation metric (e.g. Moran's I), or fragmentation index (e.g. fractal dimension). The index $f_{x,y,z}$ in different windows thus reflects spatial patterns in a particular place and at a particular scale. In other words, the PM stacks 2D spatial indices along the z-axis into a 3D matrix, where the horizontal dimensions (the x and y axes) represent the space and the vertical dimension (the z axis) represents the scale at which the indices are computed. If the windows are constrained to fit completely within a study area, the size of the layer shrinks as the window size increases, until reaching the top of the pyramid that covers the entire study area. For intuitiveness, a square study area is used in the experiment in this study. However, the PM has various configurations to represent spatial data in other tessellations (hexagons, Voronoi polygons and irregular polygons), where the coordinates of points in the 3D space (x, y, z) are defined differently to meet specific analytical purposes. Additionally, the PM can be developed in other shapes if the study area is not a square.

4. Density-based point pattern analysis in PM

4.1. Dataset

A simulated point set in a 500×500 units artificial study area is used to test the utility of the PM for point pattern analysis. These points imitate individual events such as crime incidents or disease victims distributed over geographic space. As an aside, the point values could be raw counts or ratios (for example, number of disease mortalities per 100,000 population). To create complex and multi-scale patterns, the point set is combined from four clustered point sets simulated using the Python Spatial Analysis Library (PySal; Rey & Anselin, 2007). The four clustering point sets were simulated in a Poisson cluster process. For each point set, *n* parent points are randomly distributed in the study area, and then m child points are simulated within a radius r centered around each parent. This simulation creates a known clustering pattern of the child points. By varying m, n, r, four sets of child points with different clustering patterns are generated and then

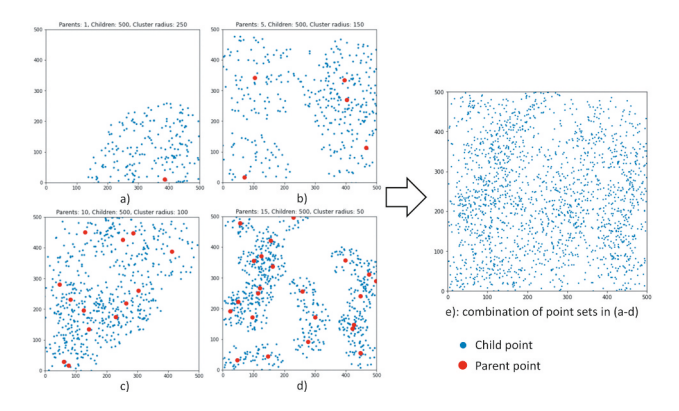


Figure 3. The simulated point set. a) - d) four clustered point sets simulated using different parameters. e) the composite point set combining a) - d).

combined by overlay into a single-point set (Figure 3). In the following analyses, the combined point set is used to test the ability of the PM for detecting multi-scale point patterns.

4.2. Representing quadrat density in PM

Quadrat density suffers effects of MAUP when choosing quadrat size, as discussed above. In this session, we demonstrate the PM representations of quadrats of the simulated point set. The configuration of the PM for quadrat density is the same as demonstrated in Figure 4. Point density is computed in square quadrats of different sizes, which are projected to points in a 3D space. Unlike the traditional quadrat analysis in a fixed tessellation, point density in the PM is computed in a moving window rolling through the point set (Figure 4(a,b)). This process is repeated for different window sizes. Next, the computed density D of each window is projected to a point (x, y, z) in the 3D PM, where x and y are the centroid of the window and z corresponds to the window size. For computation and visualization, the point lattice in the PM is implemented as a 3D matrix where each voxel represents a specific window. In other words, the construction of a PM stacks density rasters computed for different window sizes into a 3D pyramid (Figure 4(c-e)). Here, we define z as equal to half of the

z) represents a window whose centroid is at (x, y) and the side length is 2z. As such, the point density computed for all window sizes is represented by voxels in a 500*500*250 pyramid.

The result of spatial analysis often varies at different scales. Even the answer to a simple question "where are the points densest" can differ when computed at different scales. To demonstrate this phenomenon, the global density peak at each height (z) in the PM is selected and linked into a sequence. A global density peak is the position where the point density is highest when measured at a specific scale (window size). The density peak is represented by the point at (x, y, z) where (x, y)denotes the centroid of the window and z indicates the window size. Figure 5 illustrates the sequence of global density peaks measured in different window sizes, and in four different views. Altitude is the angle of the view point to the horizon. Altitude ranges from 0 degree (a horizontal, profile view) to 90 degrees (a vertical, overhead view). Azimuth is the direction of the view point along the horizon (0 degree points to the north). From the sequence in Figure 5, we can observe that the density peak constantly changes its position in the horizontal dimension (x, y), indicating that the area with the densest points is located at different positions when measured at different scales. The density peak at lower levels (small z) moves dramatically in the horizontal dimensions, implying that multiple density peaks compete for

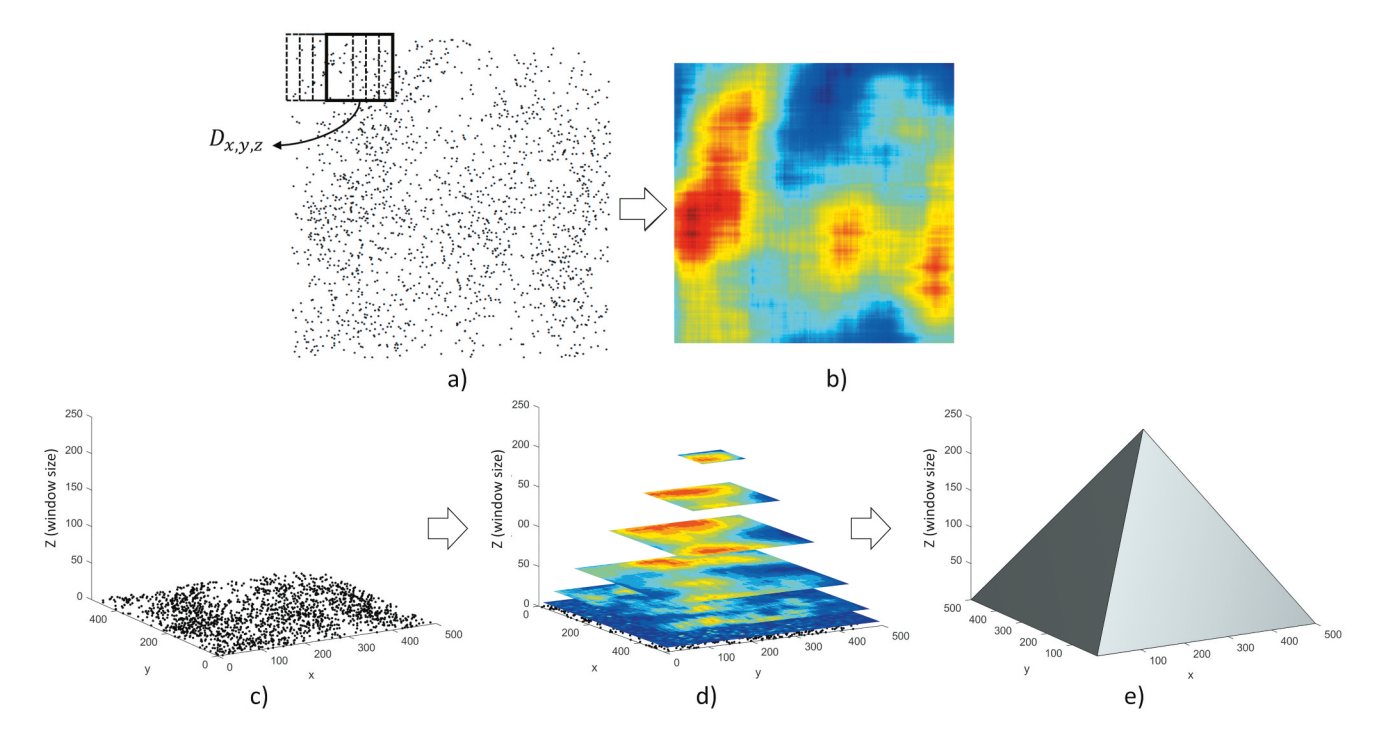


Figure 4. Representing point density in different sizes of moving windows in a 3D PM. a) moving window rolling through a point set. b) color-coded point density in moving windows. c) a point set in a 2D space. d) point density in different sizes of moving windows. e) a 3D pyramid representing all moving windows.

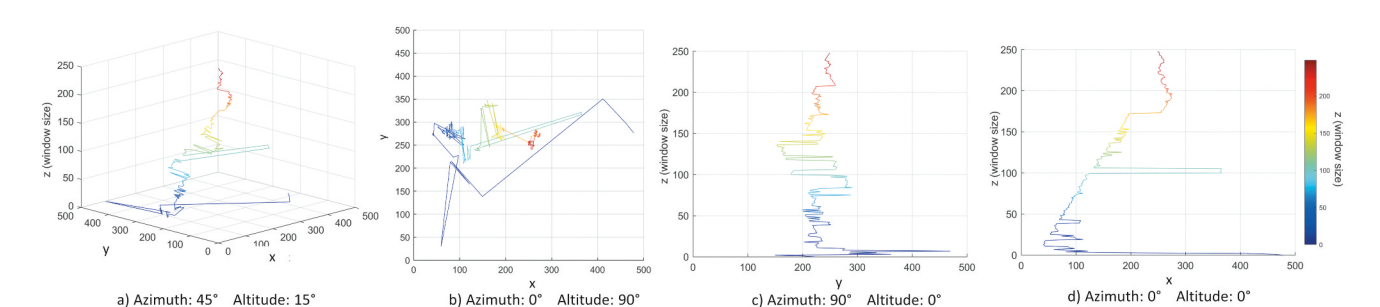


Figure 5. Sequence of the global density peak in the PM in four different view angles.

the global peak at the local scales. The horizontal position of density peak begins to stabilize as z increases, except for another large shift occurring when z is about 100, as well as some moderate shifts in the middle range. The movement of the global density peak in the PM visualizes the process of how spatial analysis result changes at different scales. It is important to note that positional shifts and extreme magnitude variations are readily apparent within the PM framework, but would be more difficult to identify exhaustively in a single-scale or selective-scale analysis. The ability to visualize, extract, and analyze progressive changes in summary statistics at different scales and locations is one of the several advantages contributed by the use of the PM framework.

In addition to the global density peak, moving windows in which the density exceeding a certain threshold can be selected and displayed as voxels in the PM. As the distribution of point density varies in different window sizes, we use percentiles as the threshold to select high-density windows. In Figure 6, voxels in the 99th percentile of point density at each z level are displayed in the PM. These voxels represent the top 1% high-density areas measured in each window size. In an interactive 3D view, one can navigate to observe the structure of the displayed voxels from different view angles. Many subtle high-density voxels are

scattered at lower z levels, indicating that many small point clusters exist at a fine scale. As the scale becomes coarser (z increases), the scattered voxels converge to larger clusters of voxels. These clusters represent spatial locations and scales where the point density is high. For example, Cluster 1 (denoted as C1) develops at fine scales, spans a wide range of scales, and disappears when z (window size) increases to 140. Analogously, C2 emerges where $z \approx 70$ and ends where z reaches 170. The long shapes of C1 and C2 indicate two point clusters that are detectable across a wide range of scales. In contrast, C3 is smaller in size and floats at medium height in the PM. This floating voxel cluster represents a point cluster that only appears within a specific range of scales and is not detectable at other scales. The isolation of C3 from other voxels means that it is formed by several point clusters at fine scales. Unlike C1 and C2 that are detectable on a wide range of scales, C1 is a kind of spatial pattern that can be easily missed in spatial analysis with randomly chosen window sizes.

4.3. Representing kernel density in PM

The configuration of PM for kernel density maps is slightly different from that for quadrat density. In a PM, kernel density maps created with different bandwidths are placed

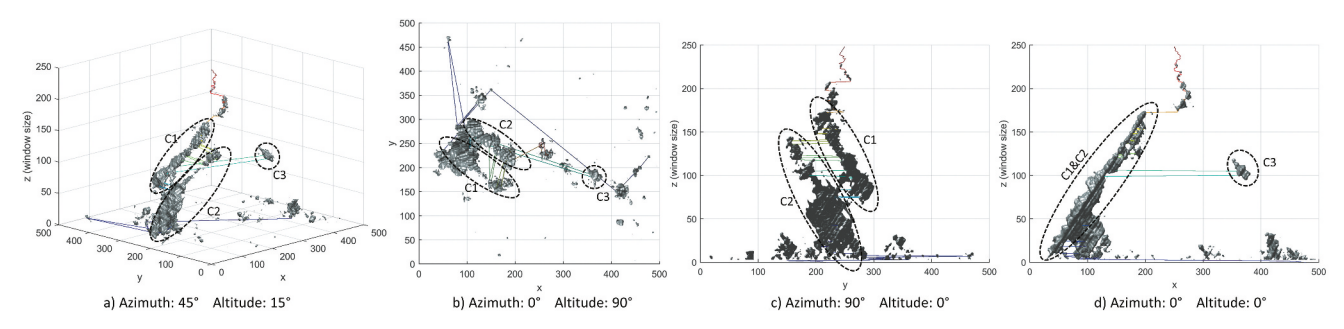


Figure 6. Voxels in the 99th percentile of point density measured in different window sizes. The colored line indicates the sequence of the global density peak as shown in Figure 5.

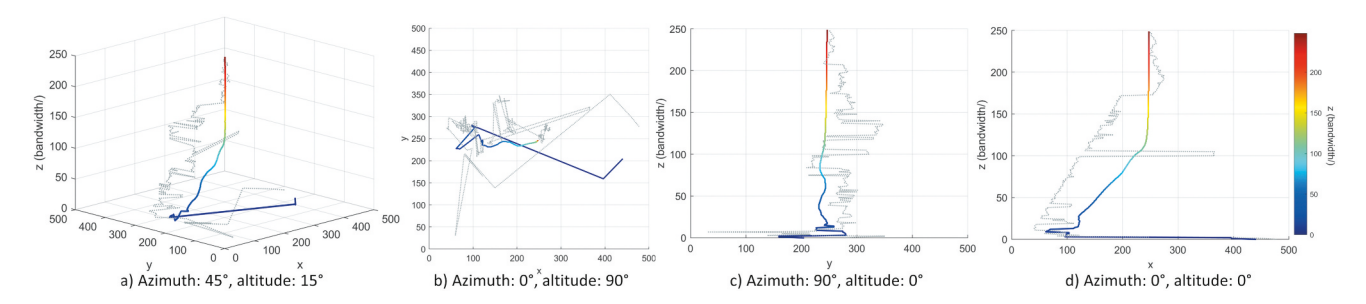


Figure 7. The color line is the sequence of global peaks in kernel density maps of different bandwidths. For comparison, the gray dotted line is the sequence of the global peaks of quadrat density shown in Figure 5.

at different heights in the 3D space. As the default function in most GIS, kernels are created using the quartic (biweight) function. In the PM, each voxel at (x, y, z)represents the kernel density computed using a specific bandwidth z at the horizontal position (x, y). As shown in Figure 7, the global density peak in a kernel density map changes with the bandwidth. The horizontal location of the density peak shifts dramatically at low z levels (small bandwidths). As z (bandwidth) increases, the density peak stabilizes and gradually moves toward the center of the study area. The global peaks of kernel density (color line in Figure 7) and quadrat density (dotted line) generally follow the same trend, both of which shift from east to west at the fine scales, and gradually move toward the center at medium and coarse scales. However, the two global peaks do not completely align due to different calculations of the two density measures. The moving window for quadrat density rolls through each location in the study area, while kernel density map aggregates kernels centered at each point. Compared with quadrat density, the global peak of kernel density is more stable with relatively fewer movements in location. In particular, at medium and coarse scales (i.e. bandwidth >50), the peak of kernel density has a very smooth transition from the eastern side to the center of the study area. This implies that spatial pattern displayed in kernel density maps is less sensitive to scale changes compared to quadrat density maps. This seems logical given that kernel density creates a continuous surface, while quadrats are discretized according to quadrat cell size. Herein lies a second benefit of the PM, namely, the capability to compare multi-scale patterns across multiple methods of computation (here, a discrete and a continuous example). Computing both metrics across single or selective scales would provide only a single snapshot or a sampling of densities, leaving the analyst to infer intermediary outcomes.

In addition to the global peak, local peaks (also known as local maxima) can reveal additional point clusters. A local peak reflects a point (x,y) where the value (i.e. density) is higher than values at the

surrounding points. As the bandwidth increases, subtle clusters at local scales are gradually smoothed out and general clusters at coarser scales start to emerge. In this study, the algorithm developed by Natan (2021) was used to detect local peaks in kernel density maps. The algorithm repeats for each bandwidth to create multi-scale kernel density maps in the PM. Local density peaks detected with different bandwidths are projected as 3D points in the PM, where (x, y) represent horizontal locations of the peaks, and z represents the bandwidths. As shown in Figure 8, most local peaks are detected at lower z levels (bandwidth <20). A few linear sequences of local peaks extend to higher z levels with changing positions in the horizontal dimension. These linear streams represent point clusters that are prominent across a wider range of scales. These streams visualize the progression of local point clusters into general clusters at a coarser scale and create linkages between local-scale and large-scale clusters. The length of the streams in the z-dimension indicates the range of scales (bandwidths) within which the point clusters are detectable, effectively highlighting the most dominant clusters in the pyramid.

Figure 9 displays voxels with a density in the 99th percentile measured in each bandwidth (z). These voxels represent high-density areas detected at different scales. Unlike Figure 6 for quadrat density, the high-density voxels of kernel density are in smoother shapes and linearly extend along the z-dimension. At fine scales (z < 10), the high-density voxels are scattered at different positions in the horizontal dimensions, which represent many clusters detected at finer scales. As the z (bandwidth) increases, the scattered voxels disappear, leaving only a cylinder of voxels around the density peak. The PM provides a complete view of the evolution of the point pattern across different scales. For example, when zooming in to lower z levels ($0 \le z \le 30$; Figure 9 (b-e)), one can observe the locations of point clusters as well as the range of bandwidths where these clusters are

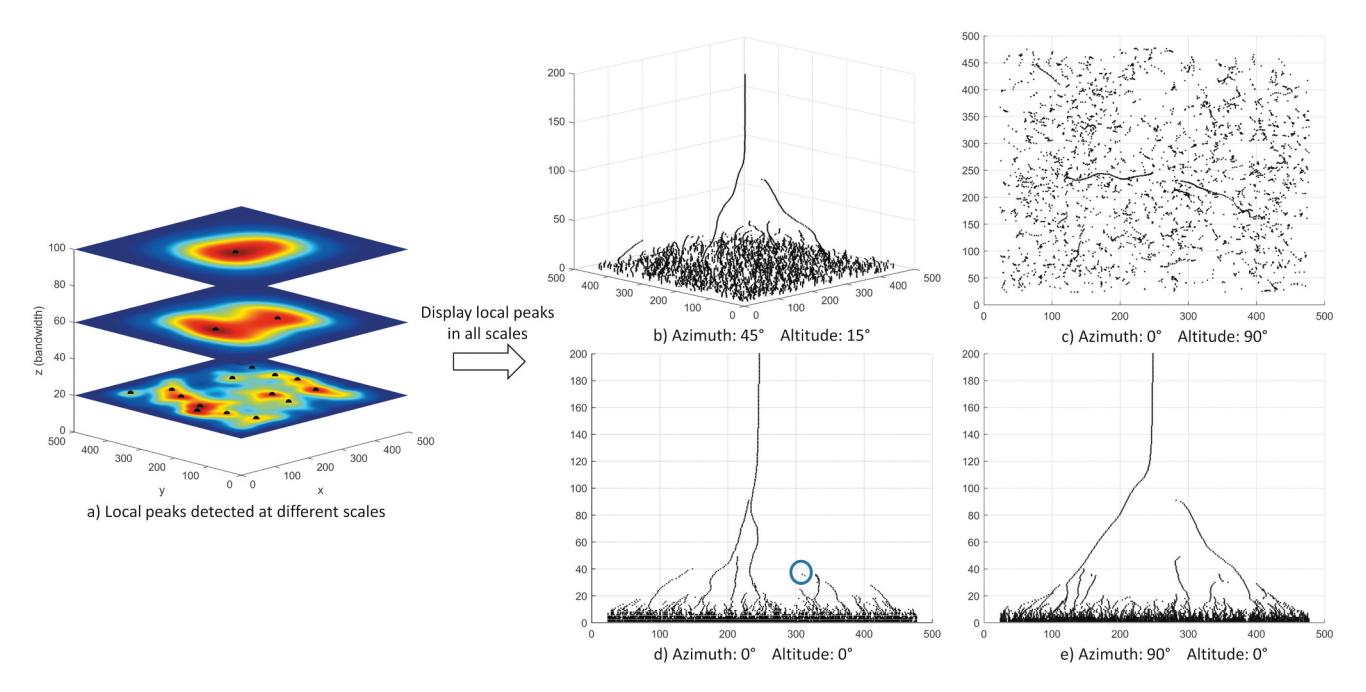


Figure 8. Visualizing local peaks of kernel density at different scales in the PM. a) local peaks detected in kernel density maps created with three different bandwidths. b) – e) local peaks detected in kernel density maps in all bandwidths: b) Azimuth: 45°, altitude: 15°; c) Azimuth: 0°, altitude: 90°; d) Azimuth: 90°, altitude: 0°; e) Azimuth: 0°, altitude: 0°.

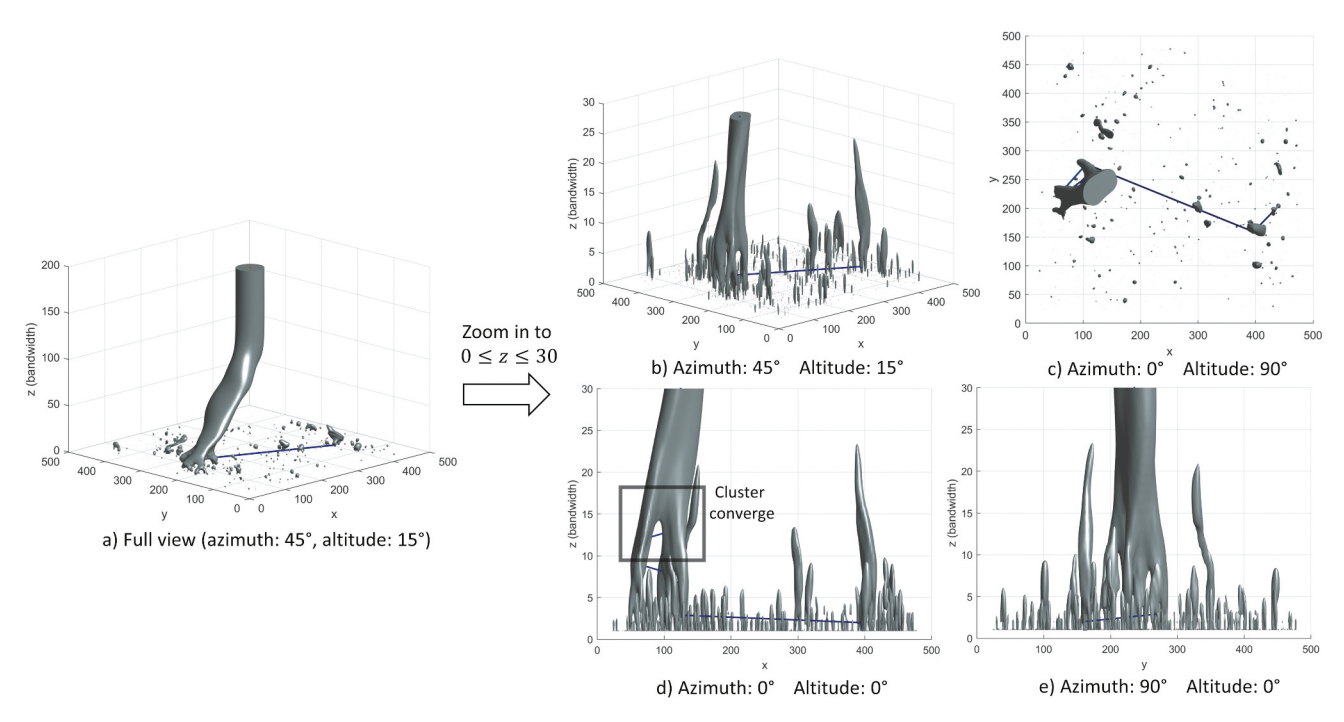


Figure 9. Voxels with a density in the 99th percentile at each scale. a) the full view at an oblique view angle. b) – e) zoomed-in views to local scales ($0 \le z \le 30$) with linearly stretched z axis.

detectable. Additionally, one can observe how the local clusters disappear or converge to general clusters in a continuous view. As an example, the box in Figure 9(d) highlights a convergence of several small clusters to a general cluster at a coarser scale.

In addition to navigating in the 3D environment, interactive controls have been developed to adjust the visualization parameters. For example, a kernel density map with a specific bandwidth can be added to the PM (Figure 10(a)). Using a slider, the kernel density map

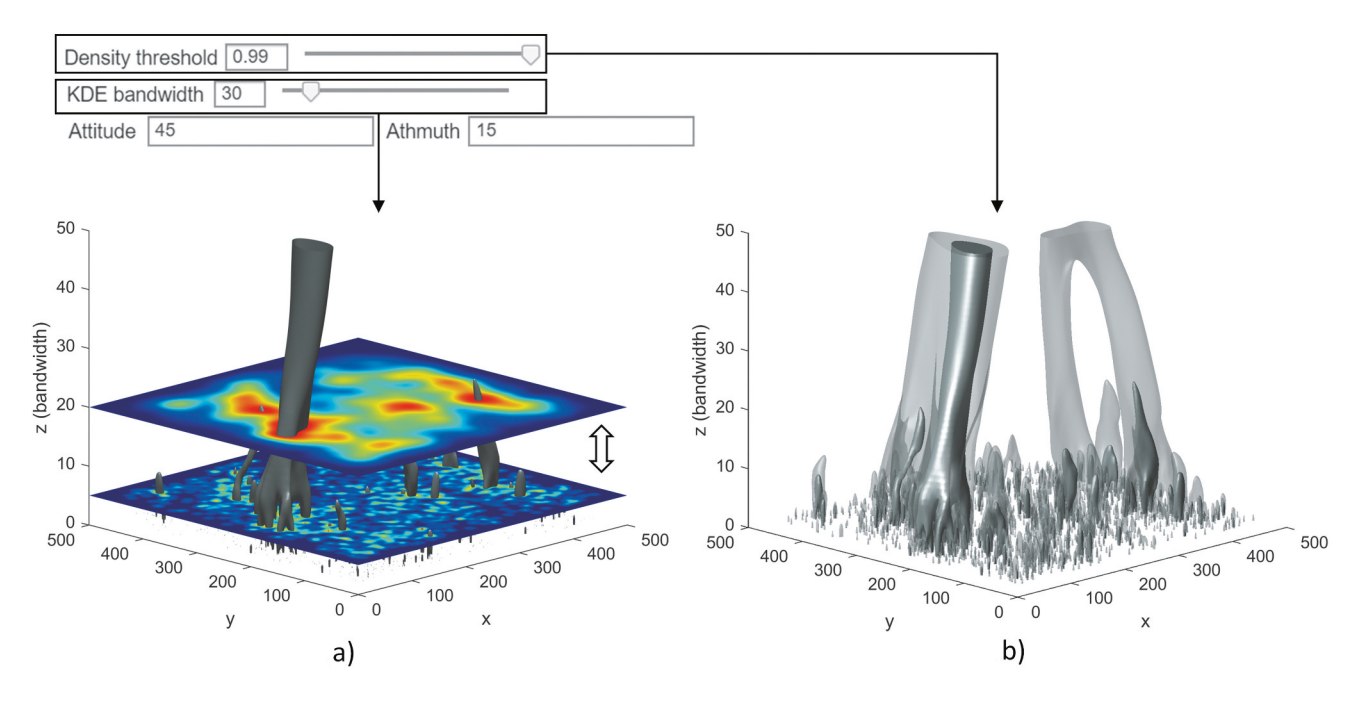


Figure 10. Using interactive controls to adjust visualization parameters. a) adding and moving kernel density maps in the PM. b) adjusting the selection threshold of high-density voxels. The solid volumes are voxels with a density in the 99th percentile, while the semitransparent volumes are voxels in the 95th percentile.

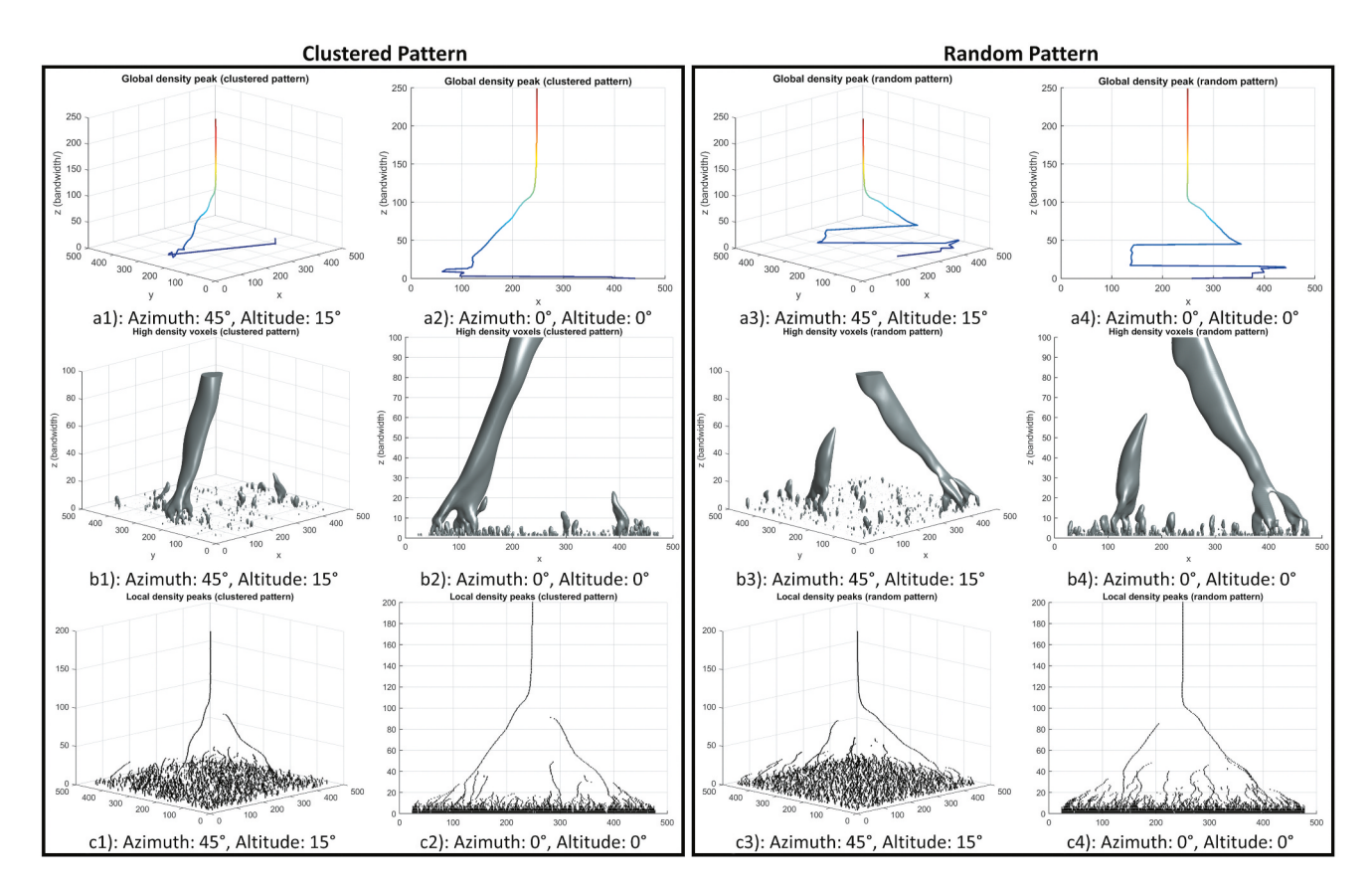


Figure 11. Comparing the PM representation of kernel density between the simulated point set and a random point set at two different view angles. a1) - a4) global density peak of kernel density; b1) - b4) 99^{th} percentile high-density voxels; c1) - c4) local density peaks.

can move to different z-values, showing density patterns computed with different bandwidths. Combining the kernel density map with the PM provides an intuitive transition from a kernel density map to its multi-scale representation in the PM. It also allows users to observe the continuous progression of clustering patterns across scales and the hierarchy between the clusters. Additionally, the threshold can be adjusted to select voxels with a density of different percentiles (Figure 10(b)). The higher the threshold being selected, the smaller the volume of voxels is displayed in the PM, representing locations where the point density is above the threshold. In such a way, users can choose appropriate thresholds to detect point clusters and observe the distribution of detected clusters at different scales.

4.4. Comparing random and clustered pattern

In order to explore the inferential potential of the PM, we compared the PM visualization of kernel density between the simulated point set and a random point set with the same number of points. As shown in Figure 11(a1-4), the global density peak of the clustered point set stabilized quickly at a fine scale (small bandwidth), while the global peak of the random point set shows dramatic shifts until reaching a coarser scale (bandwidth ≈ 50). The 99th high-density voxels of the clustered point set are more concentrated, which results in a major column extending from finer scales to coarse scales (Figure 11(b1&2)). In contrast, the high-density voxels of the random set tend to appear at multiple locations Figure 11(b3&4), and these voxels converge to a single column at a higher level. The local density peaks of the random point set (Figure 11(c1&c2)) show longer linear streams than those of the clustered set (Figure 11(c3&c4)). Figure 12 shows that local density peaks and the standard deviation of the density of both point sets decline as the scale becomes coarser. However, the clustered point set has fewer local density peaks and larger standard deviation than the random set at all scales, and the differences are most prominent

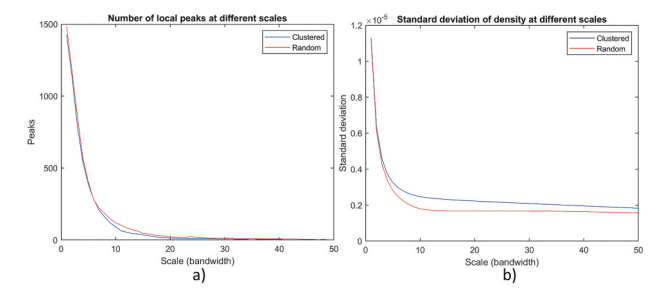


Figure 12. Number of local density peaks and standard deviation of kernel density at different scales.

when the bandwidth is around 10. These comparisons provide preliminary evidence of the inferential power of the PM in differentiating processes behind the observed patterns. However, more research is needed to identify metrics that can be used for statistical testing and develop a formal framework to infer and measure spatial processes.

4.5. Computational aspects

The point sets used in the study were generated using PySal package in Python. Due to fast and stable 3D rendering capacities, Matlab* was chosen as a platform to implement the 3D visualization of the PM. Matlab can visualize a variety of vector and raster features in an integrated 3D view. Visualization tools (e.g. volume display, isosurfaces, and slices) built on Matlab are applied to display vector and raster features extracted from the PM. Visualization tools (e.g. volume display, isosurfaces, and slices) built on Matlab are applied to display vector and raster features extracted from the PM.

The computing environment was a desktop computer with a 12-core CPU at 3.65 GHz, 128GB RAM and an AMD Radeon Pro WX 3200 graphics card. Most of the computational load is on the calculation of multiscale density in the PM. Using a sequential program, the computer takes 40 seconds to generate a PM for kernel density and 50 minutes for a quadrat density PM. The slower computing time for the quadrat density can be attributed to the "for loops" used to calculate density in different moving windows and bandwidths. The data size of a PM model ($500 \times 500 \times 250$) in this study is ~500 MB. Once the multi-scale density in PM is computed, the rendering time of the 3D visualization is trivial. In Matlab, all the demonstrated visualization can be rendered within 5 seconds.

Still, the algorithm and data structure of the PM still have room for optimization. First, since the density measures at different scales can be computed independently of each other, parallel programs can be applied to accelerate the processing of the PM on multi-core or Graphics Processing Unit (GPU) processors. Second, since the computation of a PM includes repetitive processing of overlapped data subsets, the algorithm can be further sped up via dynamic programming or by preprocessing of the input data and storing (partial) results for future reuse. Third, the data size can be reduced by storing the PM in kd-trees, quad-trees, or R-trees, which have been successfully used in other geospatial applications. These optimization options will be explored in the future research. As a proof of concept in

Matlab, we will develop the visualization tools in open-source platforms (such as Python and R) to facilitate research sharing and reproducibility.

5. Discussion

This article implements a Pyramid Model data framework (PM) in a 3D environment and applies a suite of 3D visualization techniques to analyze point patterns at multiple scales. Unlike traditional spatial analysis usually conducted at a single scale or a few discrete scales, the PM integrates space and scale in a 3D view to represent the continuous variation of spatial pattern across multiple scales. This study uses two density-based measures (quadrat density and kernel density) to evaluate the utility of the PM in multi-scale spatial analysis. The visualization of the global and local density peaks in the 3D space explicitly displays the varying locations of point clusters at different scales. Additionally, point clusters detected with various scaling parameters (quadrat size and bandwidth) are visualized as 3D voxels in the PM. The distribution of the voxels indicates locations and scales where point clusters can be detected and demonstrates the process of how local clusters evolve to general clusters at a courser scale.

Existing multi-scale analytical approaches tend to treat space and spatial scale as separate variables, controlling one variable and analyzing the change in the other variable. The PM improves upon the conventional representation by integrating space and spatial scale in a 3D environment, which is analogous to the idea of a space-time cube that combines space and time in a 3D space. Advances in computing techniques enable efficient visualization of 3D vectors and volumes, which lays a foundation for modifying conventional statistical tools for implementation in the PM. As demonstrated in the point pattern analysis reported in this study. The PM provides a new perspective to analyze multi-scale spatial patterns. The global and local density peaks visualized in the 3D space explicitly show the varying locations of point clusters when computed at different scales, demonstrating the potential of the PM as a platform to understand and measure scale sensitivity of spatial metrics. The high-density voxels vividly show a continuous progression of point pattern densities across multiple scales. These visualizations combine "snapshots" of spatial patterns at discrete scales in a unified view that can explicitly display nested relations and hierarchical structures of multiscale patterns. The PM provides a novel framework to facilitate the comprehension and analysis of multiscale spatial patterns and relations. Overall, this article demonstrates how a linked and hierarchical data framework (the PM) can offer increased analytical power to detect, identify, and explore fine- and coarse-scale insights about point pattern densities and clustering.

One aspect of multi-scale point pattern analysis is to develop general and specific conclusions about the spatial processes that generate the point data. While it is widely acknowledged in the geospatial disciplines that such generating processes operate within specific scale ranges, there is at present no catalog or inventory of what processes emerge at particular scales, beyond rough estimates. In physical processes, for example, it is known that isostatic rebound is evident at continental but not local scales, while erosion and deposition tend to emerge at local or regional but not continental scales. In social processes, similar analogies can be drawn about land cover as opposed to land use, while some processes such as migration can be detected at local, regional, and global scales. These scale categories (local, regional, etc.) are discursive, however, and not precisely quantifiable. Because the PM provides metrics as well as visualization across a range of scales, the data framework affords the opportunity to search for a more precise quantification of the scale at which specific spatial patterns emerge or disappear. While the research reported here does not make that demonstration, the potential is evident and this forms an interesting direction for future work. Furthermore, machine learning techniques can be applied to associate patterns in the PM with different spatial processes. The current outcomes point to several additional directions for further development as discussed below.

First, further research is needed to develop inferential functions of the PM. Section 4.4 presents a preliminary analysis to compare the PM visualizations between a random point set and the synthetic clustering point set, which exhibit distinct patterns in the PM. In future research, such differences could be systematically analyzed in a Monte Carlo simulation. By comparing meaningful metrics in the PM, a formal framework can be developed to implement inferential testing. In addition to detecting prominent patterns at different scales, spatial models can be built in the PM framework to quantify multi-scale relations between predictive and dependent variables. Unlike simple visualizations that may sometimes be influenced by analysts' subjective opinions, the quantitative methods will provide reliable metrics to detect, classify, and rank multi-scale spatial patterns in the PM. Further exploration is needed to fully realize the potential of the PM in analyzing other spatial metrics. One area of work is mentioned earlier in the paper that (in addition to raw or absolute data values) the PM can

represent the ratio between a variable and associated background variables such as point event density and population density to account for non-homogenous population background, which is a common issue in many geographic domains, for example, in disease analysis and monitoring (Shi, 2010). Additionally, the PM framework is applicable to other scale-sensitive spatial indices, such as spatial autocorrelation (e.g. Moran's I), GWR coefficients, accuracy of image classification and land cover change prediction (Carlson et al., 2020). Work on modifying conventional calculations for these methods and to prepare them for implementation in the PM framework is underway.

A possible limitation of this work is that the novel visualization of the PM may inevitably introduce extra cognitive load to viewers. The issue also exists in other geovisualization platforms where the controversies about 2D vs. 3D and static vs. animated are far from settled. For example, most critiques of the space-time cubes and aquariums popularized in Time Geography (Hägerstraand, 1970; Kwan, 2004; Miller, 1991) centered on cognitive challenges and usability in specific analytical tasks. However, these critics did not prevent the visualization methods from becoming a profound concept in geography and a widely used visualization platform in GIS. To resolve such issues in the PM, empirical assessments need to be conducted to collect user feedback and evaluate the usability of the PM in different analytical tasks. Usability might be assessed in the context of how much training time is needed before scholars can effectively use the PM-based tools to analyze data. New visualization techniques, such as linked views, controlled animation, and augmented reality, can be applied to the PM to minimize the cognitive load and facilitate human users to utilize the PM for analytical tasks.

Another limitation of this work is the processing time required to reformat spatial data for input to a PM, as well as to prepare modeling and visualization outcomes for summary and display. The present experiments are displayed using Matlab, a proprietary platform. Acknowledging that open-source languages create a better option for research sharing and reproduction, the authors originally tried to develop visualizations using Python packages including Plotly and Mayavi. However, these packages have several technical challenges. For example, both packages are slow in rendering 3D isosurfaces and often crash when changing the view, creating impediments for real-time data exploration. Additionally, it was difficult to use the Python packages to plot different types of 3D objects (points, lines, slices, and volumes) within the same view. To this

end, the authors chose Matlab at this experimental stage. In the future, after optimization of data structure and algorithms, tools will be implemented in Python.

6. Conclusion

The major contributions of this work can be summarized as follows. First, this study demonstrates the potential of the PM in advancing multi-scale spatial analysis and modeling. The integrated view of space and scale allows users to observe and to quantify nested relations between spatial patterns at different scales and understand the scaling issue and MAUP in spatial analysis. Second, this study demonstrates the use of 3D visualization techniques, including interactive animation, to analyze the PM. Unlike traditional spatial data usually represented in a 2D space, the PM requires a new suite of analytical tools, essentially modifying and expanding the conventional computations, that can explore the internal patterns in 3D volumes. This study shows how the existing 3D visualization tools (e.g. volume display, isosurfaces, and slicing) can be applied to analyze multi-scale spatial patterns in the PM. Third, as the issue of scale exists in spatial and temporal data as well as spatio-temporal data, the research on models lays a foundation for developing new visualization and analytical tools that support multi-scale spatiotemporal analysis.

Acknowledgments

The authors would like to express their sincere gratitude to the anonymous reviewers and Dr. Eric Delmelle for their constructive feedback, which ultimately improved the quality of this manuscript.

Disclosure statement

No potential conflict of interest was reported by the author(s).

Funding

This article is based on work supported by two research grants from the U.S. National Science Foundation: one under the Methodology, Measurement & Statistics (MMS) Program (Award No. 2102019) and the other under the Coastlines and People (CoPe) Program (Award No. 2052063). Any opinions, findings, and conclusions or recommendations expressed in this material are those of the authors and do not necessarily reflect the views of the funding agencies.



ORCID

Yi Qiang http://orcid.org/0000-0002-6872-8837 Barbara Buttenfield http://orcid.org/0000-0001-5961-5809 Jinwen Xu http://orcid.org/0000-0001-9663-5737

Data Availability Statement

The data and software that support the findings of this study are available with the identifier(s) in a Github repository (https://github.com/qiang-yi/PM).

References

- Behrens, T., Viscarra Rossel, R. A., Kerry, R., MacMillan, R., Schmidt, K., Lee, J., Scholten, T., & Zhu, A.-X. (2019). The relevant range of scales for multi-scale contextual spatial modelling. Scientific Report, 9(1), 14800. https://doi.org/10. 1038/s41598-019-51395-3
- Carlson, K., Buttenfield, B., & Qiang, Y. (2020). Visualizing uncertainty metrics across multiple attribute resolutions [Presentation]. AutoCarto 2020, virtual conference.
- Chen, L., Gao, Y., Zhu, D., Yuan, Y., & Liu, Y. (2019). Quantifying the scale effect in geospatial big data using semi-variograms. PLOS ONE, 14(11), e0225139. https:// doi.org/10.1371/journal.pone.0225139
- Chica-Olmo, M., & Abarca-Hernández, F. (2000). Computing geostatistical image texture for remotely sensed data classification. Computers & Geosciences, 26 (4), 373-383. https://doi.org/10.1016/S0098-3004(99) 00118-1
- Diggle, P., Rowlingson, B., & Su, T. (2005). Point process methodology for on-line spatio-temporal disease surveillance. Environmetrics, 16(5), 423-434. https://doi. org/10.1002/env.712
- Duque, J. C., Laniado, H., & Polo, A. (2018). S-maup: Statistical test to measure the sensitivity to the modifiable areal unit problem. PLOS ONE, 13(11), e0207377. https:// doi.org/10.1371/journal.pone.0207377
- Ester, M., Kriegel, H.-P., Sander, J., & Xu, X. (1996). A density-based algorithm for discovering clusters in large spatial databases with noise. Proceedings of the second international conference on knowledge discovery and data mining, KDD'96 (pp. 226-231). AAAI Press.
- Fotheringham, A. S., Yang, W., & Kang, W. (2017). Multiscale Geographically Weighted Regression (MGWR). Annals of American Association of Geographers, 107(6), 1247-1265. https://doi.org/10.1080/ 24694452.2017.1352480
- Gatrell, A. C., Bailey, T. C., Diggle, P. J., & Rowlingson, B. S. (1996). Spatial point pattern analysis and its application in geographical epidemiology. Transactions of the Institute of British Geographers, 21(1), 256-274. https://doi.org/10. 2307/622936
- Hägerstraand, T. (1970). What about people in regional science? Papers in Regional Science, 24. https://doi.org/10. 1111/j.1435-5597.1970.tb01464.x

- Kraak, M.-J. (2003). The space-time cube revisited from a geovisualization perspective. Proceedings of the 21st international cartographic conference (pp. 1988-1996). International Cartographic Association.
- Kulldorff, M. (1997). A spatial scan statistic. Communications in Statistics - Theory and Methods, 26(6), 1481-1496. https://doi.org/10.1080/03610929708831995
- Kwan, M.-P. (2004). GIS methods in time-geographic research: Geocomputation and geovisualization of human activity patterns. Geografiska Annaler: Series B, Human Geography, 86(4), 267-280. https://doi.org/10.1111/j.0435-3684.2004.00167.x
- Lam, N. S.-N. (1983). Spatial Interpolation Methods: A Review. The American Cartographer, 10(2), 129-150. https://doi.org/10.1559/152304083783914958
- Lam, -N. S.-N., Cheng, W., Zou, L., & Cai, H. (2018). Effects of landscape fragmentation on land loss. Remote Sensing of Environment, 209, 253-262. https://doi.org/10.1016/j.rse. 2017.12.034
- Miller, H. J. (1991). Modelling accessibility using space-time prism concepts within geographical information systems. International Journal of Geographical Information Systems, 5(3), 287-301. https://doi.org/10.1080/02693799108927856
- Mills, P. (2011). Efficient statistical classification of satellite measurements. International Journal of Remote Sensing, 32(21), 6109-6132. https://doi.org/10.1080/01431161.2010.507795
- Natan, A. (2021, May 26). Fast 2D peak finder. https://github. com/adinatan/fastpeakfind/releases/tag/1.13.0.0
- O'Sullivan, D., & Unwin, D. (2010). Chapter 4: Point pattern analysis. In Geographic information analysis. (pp. 121-155). New Jersey: John Wiley & Sons, Inc., Hoboken.
- Openshaw, S. (1983). The modifiable areal unit problem. In Concepts and Techniques in Modern Geography, 38. Norwich, UK: Geo Books.
- Qiang, Y., Buttenfield, B. P., Lam, N., & De Weghe, N. V. (2018). Novel models for multi-scale spatial and temporal analyses. In S. Winter, A. Griffin, & M. Sester (Eds.), 10th International Conference on Geographic Information Science (GIScience 2018), Leibniz International Proceedings in Informatics (LIPIcs) (pp. 55:1-55:7). Schloss Dagstuhl-Leibniz-Zentrum fuer Informatik. https://doi.org/10.4230/ LIPIcs.GISCIENCE.2018.55.
- Qiang, Y., Chavoshi, S. H., Logghe, S., De Maeyer, P., & Van De Weghe, N. (2014). Multi-scale analysis of linear data in a two-dimensional space. Information Visualization, 13(3), 248-265. https://doi.org/10.1177/1473871613477853
- Qiang, Y., & Van de Weghe, N. (2019). Re-arranging space, time and scales in GIS: Alternative models for multi-scale spatio-temporal modeling and analyses. International Journal of Geo-Information, 8(2), 72. https:// doi.org/10.3390/ijgi8020072
- Rey, S. J., & Anselin, L. (2007). PySAL: A python library of spatial analytical methods. The Review of Regional Studies, 37(1), 5-27. https://doi.org/10.52324/001c.8285
- Shi, X. (2010). Selection of bandwidth type and adjustment side in kernel density estimation over inhomogeneous backgrounds. International Journal of Geographical Information Science, 24(5), 643-660. https://doi.org/10. 1080/13658810902950625
- Silverman, B. W. (1986). Density estimation for statistics and data analysis. Chapman & Hall.



- Terrell, G. R., & Scott, D. W. (1992). Variable kernel density estimation. *The Annals of Statistics*, 20(3), 1236–1265. https://doi.org/10.1214/aos/1176348768
- Tiwari, C., & Rushton, G. (2005). Using spatially adaptive filters to map late stage colorectal cancer incidence in Iowa. In P. F. Fisher (Ed.), *Developments in spatial data handling* (pp. 665–676). Springer. https://doi.org/10.1007/3-540-26772-7_50
- Tiwari, C., & Rushton, G. (2010). A spatial analysis system for integrating data, methods and models on environmental risks and health outcomes. *Transactions in GIS*, 14, 177–195. https://doi.org/10.1111/j.1467-9671.2010.01220.x
- Van Kerm, P. (2003). Adaptive kernel density estimation. *The Stata Journal*, 3(2), 148–156. https://doi.org/10.1177/1536867X0300300204
- Wagner, H. H., & Fortin, M.-J. (2005). Spatial Analysis of Landscapes: Concepts and Statistics. *Ecology*, 86(8), 1975–1987. https://doi.org/10.1890/04-0914

- Wu, F. (2002). Calibration of stochastic cellular automata: The application to rural-urban land conversions. *International Journal of Geographical Information Science*, *16*(8), 795–818. https://doi.org/10.1080/13658810210157769
- Ye, X. (2021). Estimating σ2 for the Classical Linear Regression Model (CLRM) with the presence of the Modifiable Areal Unit Problem (MAUP). *Geographical Analysis*. https://doi.org/10.1111/gean.12291
- Ye, X., & Rogerson, P. (2021). The impacts of the Modifiable Areal Unit Problem (MAUP) on omission error. *Geographical Analysis*. 54(1), 32–57. https://doi.org/10.1111/gean.12269
- Yin, P. (2020). Kernels and density estimation. In J. P. Wilson (Ed.), *The geographic information science & technology body of knowledge* (1st Quarter 2020 ed.). https://doi.org/10.22224/gistbok/2020.1.12
- Yuan, Y., Qiang, Y., Bin Asad, K., & Chow, E. (2020). Point pattern analysis. In J. P. Wilson (Ed.), *The geographic information science & technology body of knowledge*. https://doi.org/10.22224/gistbok/2020.1.13